Published in final edited form as:

ACS Appl Mater Interfaces. 2020 April 08; 12(14): 16088–16096. doi:10.1021/acsami.0c01241.

Supramolecular Hydrogels Based on Nanoclay and Guanidine-Rich Chitosan: Injectable and Moldable Osteoinductive Carriers

Xiao Zhang[†], **Jiabing Fan**[†], **Chung-Sung Lee**[†], **Soyon Kim**[†], **Chen Chen**[†], **Min Lee**[*,†,‡]

[†]Division of Advanced Prosthodontics, University of California at Los Angeles, 10833 Le Conte Avenue, Los Angeles, California 90095, United States

[‡]Department of Bioengineering, University of California at Los Angeles, 420 Westwood Plaza, Los Angeles, California 90095, United States

Abstract

Supramolecular hydrogels have great potential as biomaterials for tissue engineering applications or vehicles for delivering therapeutic agents. Herein, a self-healing and pro-osteogenic hydrogel system is developed based on the self-assembly of laponite nanosheets and guanidinylated chitosan, where laponite works as a physical crosslinker with osteoinductive property to form a network structure with a cationic guanidine group on chitosan chains. The hydrogels can be prepared with varying ratios of chitosan to laponite and display self-healing and injectable properties due to supramolecular forces as well as osteoinductive activity due to nanoclay. They enhance cell adhesion and promote osteogenic differentiation of mesenchymal stem cells by activating the Wnt/β-catenin signaling pathway. In addition, the hydrogel is used as a malleable carrier for demineralized bone matrix (DBM). The loading of DBM does not affect the self-healing and injectable natures of hydrogels while enhancing osteogenic capacity, indicating advanced allograft bone formulations with carriers can facilitate handling and bone healing. This work provides the first demonstration of therapeutic supramolecular design for the treatment of bone defects.

Graphical Abstract

[*]**Corresponding Author:** leemin@ucla.edu. Phone: +1-310-825-6674. Fax: +1-310-825-6345.

Supporting Information. Additional data, Figures S1–S14 and Table S1. This material is available free of charge via the Internet at http://pubs.acs.org.

The authors declare no competing financial interest.

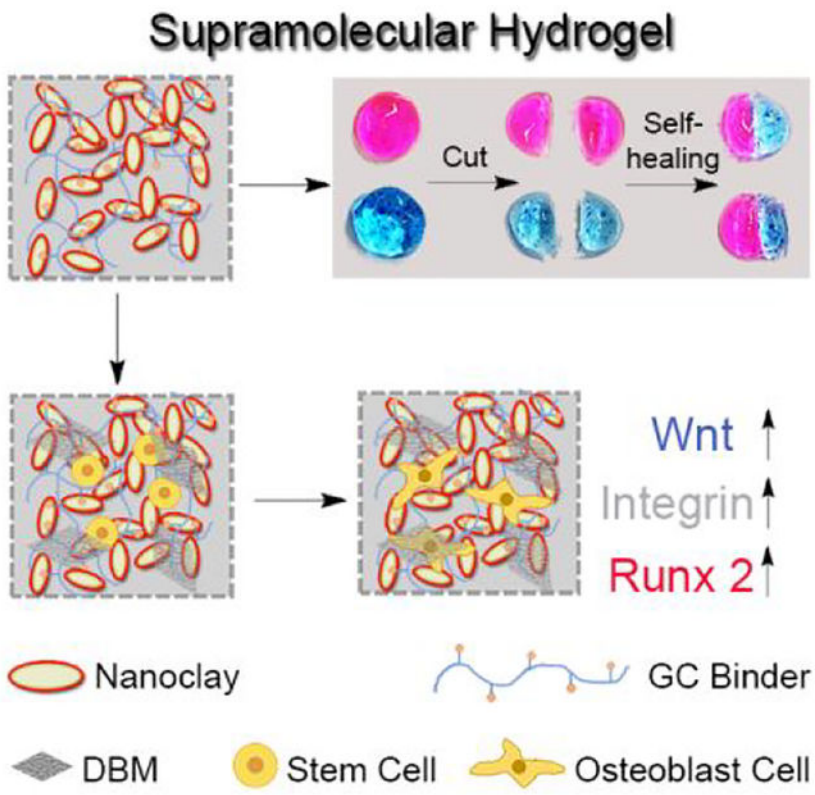

Keywords

supramolecular hydrogels; nanoclay; chitosan; osteogenesis; demineralized bone matrix

1. INTRODUCTION

Hydrogels, networks of hydrophilic polymer chains, have received great attention in regenerative medicine for use as tissue engineering scaffolds and carriers of therapeutic cells or drugs.[1–7] Traditional hydrogels are fabricated by various chemical reactions (e.g. Michael type addition, condensation reactions), radical polymerization or high energy irradiation to form crosslinked networks in aqueous solutions.[8–11] However, crosslinking agents and chemical reactions used in conventional gel formation may have detrimental effects on living cells and bioactive molecules.[9] Moreover, hydrogel networks created by chemical crosslinking are not injectable and do not recover after rupture.[12–14] On the contrary, supramolecular hydrogels are driven by reversible non-covalent bonds, including ionic interactions, hydrophobic interactions hydrogen bonding, and possess self-healing and injectable properties due to their dynamic bonding nature. These are critical features for tissue engineering applications.[11, 15–18]

Nanoclays are two-dimensional (2D) inorganic silicate particles and have been shown to be able to form supramolecular gel networks from various hydrogel precursors with self-healing nature and shape-memory behavior.[19–22] Laponite ($Na^{+}_{0.7}[(Mg_{5.5}Li_{0.3})Si_8O_{20}(OH)_4]^{-}_{0.7}$), is a synthetic disk-shaped smectite approximately 25

nm in diameter and 0.92 nm in thickness.[23] The degradation products of laponite (e.g. magnesium, lithium and orthosilicic acid) have been shown to induce osteogenic differentiation of mesenchymal stem cells and promote bone formation by regulating cell adhesion and the Wnt/β-catenin signaling pathway.[23–30] The incorporation of laponite into various polymer matrices (e.g. chitosan, PEG, PEO) not only enhanced the mechanical properties of nanocomposite hydrogels but also stimulated osteogenic differentiation even without supplementation of growth factors.[31–34]

In this work, we demonstrate a therapeutic supramolecular assembly of chitosan and nanoclays for bone regeneration applications (Figure 1). Novel supramolecular hydrogel networks are assembled from laponite nanosheets (LNSs) and guanidinylated chitosan (GC) binder via formation of salt-bridge between guanidine ion pendants in the GC binder and oxyanions on the LNS surface. These networks have several key features: (i) they are a simple and nontoxic system suitable for biomedical applications, (ii) they have injectable and self-healing features for the administration in a minimally invasive manner and the integration to the defect site without hydrogel fragmentation, (iii) they demonstrate an intrinsic osteoinductive nature and enhanced bone healing. We also demonstrate the potential of supramolecular hydrogels as malleable carriers for bone graft materials such as demineralized bone matrix (DBM) to enhance osteogenic capacity.

2. MATERIALS AND METHODS

2.1. Chemical and Materials.

Glycol chitosan, 1H-Pyrazole-1-carboxamidine hydrochloride, N, N-Diisopropylethylamine (DIPEA), sodium polyacrylate (ASAP), rhodamine, methylene blue, 5-bromo-4-chloro-3-indoxylphosphate (BCIP), Nitro Blue tetrazolium (NBT), Alizarin red S, L-ascorbic acid, p-nitrophenol phosphate, β-glycerophosphate, dexamethasone were purchased from Sigma Aldrich (St.Louis, MO). Laponite XLG was obtained from Best of Chemicals (Shirley, NY). alamarBlue™, Dulbecco's modified Eagle's medium (DMEM), fetal bovine serum (FBS), penicillin/streptomycin (P/S), Trizol reagents, cDNA transcription kit, Calcein AM, Pico 488 Green and Ethidium homodimer (EthD-1) were purchased from Life Technologies (Grand Island, NY).

2.2. Guanidinylation of Chitosan.

The primary amino groups of glycol chitosan were guanidinylated by 1H-Pyrazole-1-carboxamidine hydrochloride. In brief, 1.0 g glycol chitosan and 3.85 g 1H-Pyrazole-1-carboxamidine hydrochloride (5 equiv, according to the number of primary amino groups) were dissolved in 20 mL deionized water. Then 4.34 mL DIPEA (5 equiv, according to the number of primary amino groups) was added and reacted for 24 h at room temperature. Subsequently, the raw product was dialyzed in a dialysis bag (MWCO 3500 Da) against deionized water to remove free 1H-Pyrazole-1-carboxamidine hydrochloride. Dialyzed product was freeze dried to obtain guanidinylated chitosan, which was confirmed by ^{1}H NMR (400 MHz, D_2O).

2.3. Preparation and Characterization of Hydrogel.

Firstly, laponite was added into deionized water with magnetic stirring (1000 rpm, 30 min). ASAP was added with stirring magnetically (500 rpm) for 10 min. Finally, guanidinylated chitosan was added and mixed by a vortex for 5 s. Different amounts of laponite and chitosan were used to obtain hydrogels with various laponite/guanidinylated-chitosan ratios. Hydrogel prepared of laponite/glycol chitosan was used as a negative control. To make them easy to see, hydrogels (laponite/guanidinylated-chitosan ratio: 3 wt %/0.5 wt %) were incubated in either rhodamine B or methylene blue solutions for 30 min to generate pink and blue hydrogels, respectively. Both pink hydrogel and blue hydrogel were cut into two pieces. One piece of pink hydrogels and one piece of blue hydrogels were touched and formed into an integrated hydrogel. Then these two healed hydrogels were incubated in phosphate buffer solutions (PBS) for 3 h to detect their stability. The new hydrogels were re-cut into two pieces. Two pieces of pink-blue hydrogels were re-joined together and formed a new hydrogel. In addition, whole pink hydrogel and blue hydrogel were touched with each other for 10 min, and transfer the new pink/blue gel into deionized water for 10 min to detect its stability. Each step was photographed.

Storage modulus (G') and loss modulus (G") of hydrogels with 3 wt % LNSs were monitored using Discovery Hybrid Rheometers HR-3 (TA Intruments). Frequency sweep of the hydrogel was performed from 0.1 to 10 Hz frequency at γ = 5.0%. Strain sweep of the hydrogel was performed from 0.02% to 300 % strain at fxed 1.6 Hz frequency to study shear-thinning properties of hydrogels. Continuous step strain sweep was performed with alternating shear strains of low (1%, 300 s)-high (300%, 300 s)-low (1%, 300 s) strain.

The degradation of hydrogels was carried out for 40 days. Hydrogels with 3 wt % LNSs were incubated at 37°C in PBS (pH 7.4) or cell culture medium (DMEM, 10% FBS, and 1% P/S), which were replaced every 5 days. At a given time, hydrogels were lyophilized for weight measurement. The present residual weight of hydrogels was calculated using the following equation: Residual gel weight = M_t/M_0*100%, where M_0 and M_t refer to the weight of hydrogels at time 0 (hydrogels did not undergo degradation) and t, respectively.

2.4. Cell Encapsulation in 3D Hydrogel.

The mouse bone marrow stromal cell line (BMSCs, D1 ORL UVA [D1], D1 cell, CRL-12424) was purchased from American Type Culture Collection (ATCC, Manassas, VA) and cultured in DMEM with 10% FBS and 1% P/S at 37°C in a humidified atmosphere containing 5% CO_2. Cell culture media DMEM, penicillin, streptomycin, and FBS were purchased from Gibco (Manassas, VA). First, 2×10^7 BMSCs were suspended in 50 μL guanidinylated-chitosan solution (5 wt%, PBS). Different volumes (from 250 to 450 μL) of laponite (5 wt%) and PBS (from 200 to 0 μL) were added maintaining a final volume of 500 μL and the mixture vortexed for 5 s immediately. 50 μL of each the resulting cell-encapsulated hydrogels was cultured with 1 mL DMEM culture medium in separate wells of a 24-well plate. The culture medium was changed every 2 days.

2.5. Cell Viability Assay.

To estimate the cytotoxicity of laponite hydrogel to BMSCs, cell viability was detected using alamarBlue™. BMSCs loaded hydrogel was cultured for 1, 3, or 7 days. Then the hydrogel was stained with 1 mM calcein AM and 2 mM EthD-1 for CLSM observation. Cells were incubated with 100 μL culture medium containing 10% alamarBlue™ for another 2 h at 37°C. The fluorescence intensity was detected by a microplate reader using 570 nm excitation and 585 nm emission. The additional cytocompatibility test was performed by placing the hydrogels in tissue culture plates (TCP) in which cells were cultured and exposed to the hydrogel samples. The hydrogel and cells were separated by 70 μm mesh inserts in culture medium. The alamarBlue™ fluorescence was measured at day 1, 4, or 7 and was normalized to untreated cells grown on TCP.

2.6. Alkaline Phosphatase (ALP) Expression and Activity.

After incubation in osteogenic medium (DMEM medium containing 10% FBS, 50 μg/mL L-ascorbic acid, 10 mM β-glycerophosphate, 1% P/S and 100 nM dexamethasone) for 3, 7 or 14 days, hydrogels were fixed using 10% formalin solution for 20 min and immersed in ALP solutions (100 mM Tris, 50 mM $MgCl_2$, 100 mM NaCl, pH 8.5) for 10 min. Then hydrogels were stained with BCIP/NBT for 2 h and imaged using an Olympus IX71 microscope (Olympus, Tokyo, Japan). For ALP activity detection, hydrogels were washed with PBS and lysed using 0.1% Tween-20 buffer at 4°C for 30 min. The supernatant was collected after centrifugation at 12000 rpm for 5 min and reacted with phosphatase substrate for 2 h at 37°C. ALP concentration was measured at a wavelength of 405 nm using a microplate reader, and values were normalized to DNA content measured using Pico 488 Green.

2.7. Mineralization Assay.

After incubation in osteogenic medium for 7, 14, or 21 days, hydrogels were stained with 0.2% Alizarin red S solution for 5 min. Once washed with PBS for 3 times, hydrogels were imaged with an Olympus IX71 microscope and quantified using acetic acid with colorimetric measurement at 405 nm. The quantitative results were normalized with the weight of the hydrogels.

2.8. Quantitative Polymerase Chain Reaction (qPCR) Analysis.

At given times, total RNA was obtained from hydrogels using Trizol reagent. Then cDNA was synthesized using a cDNA transcription kit (Invitrogen). Amplification reactions including 1 μL of cDNA template, 1 μL of primer, 8 μL of distilled deionized water and 10 μL of SYBR Green were carried out using a LightCycler 480 PCR (Indianapolis, IN) for 55 cycles. The sequences of primers are listed in Table S1.

3. RESULTS AND DISCUSSION

3.1. Preparation and Characterization of Hydrogels.

First, primary amines of glycol chitosan were guanidinylated by 1H-Pyrazole-1-carboxamidine hydrochloride and DIPEA, leading to the synthesis of GC binder.[35–37] ^1H NMR spectroscopy confirmed that the signals corresponding to the protons next to primary

amines (b, δ = 1.75 ppm) were gradually shifted downfield (b', δ = 1.83 ppm) after guanidinylation (Figure 2A).[35] After dispersed with ASAP, LNS solutions were mixed with GC binder for the preparation of hydrogels.[38–41] As shown in Figure 2B, LNS solutions could form hydrogels after interaction with GC binder for 100 s. However, the mixture of LNSs and glycol chitosan was not able to form hydrogels, indicating that there was a stronger supramolecular interaction between LNSs and GC binder after guanidinylation. When LNS amount was increased from 2.5 to 4.5 wt %, the gelation time was reduced from 220 to 5 s. Increased amounts of GC binder could also decrease gelation time, indicating that the formation of hydrogels was affected by supramolecular interactions including hydrogen bonding and electrostatic interaction between LNSs and GC binder (Figure S1–S4). Meanwhile, glycol chitosan without guanidinylation was used as a control group (Figure S5). Hydrogels consisting of LNSs and glycol chitosan at a ratio of 4.0 wt %/0.5 wt % formed slower (90 s) than LNSs/GC hydrogels with the same ratio (10 s), due to the weaker supramolecular interactions between LNSs and glycol chitosan.

Next, the self-healing ability of LNSs/GC hydrogels was evaluated using the macroscopic method.[42–43] After staining with rhodamine B and methylene blue, hydrogels with two different colors were cut into two pieces and held together along the cut surface at 25°C without any external intervention. The boundaries between different pieces had blurred after 10 min and the two pieces were completely merged into a single object. Furthermore, newly formed hydrogels could maintain their shape and integrity in aqueous environment up to 3 h. After the second cut, the two pieces of pink-blue hydrogels also could form an integral new hydrogel again. (Figure 2C). Consistently, two uncut dyed hydrogels also fused into one object, and the fused hydrogels could also keep their shape and integrity in aqueous environment (Figure 2D). These results manifested that our supramolecular hydrogels exhibited excellent self-healing ability thanks to dynamic non-covalent bonds in the hydrogel networks (Figure 2E). In addition, hydrogels with injectable properties have the potential for minimally invasive therapies.[44–46] Our newly fabricated hydrogels, using various amounts of LNSs (2.5 to 4.5 wt %) exhibited an injectable feature, shown as a rapid reassembly when extruded them into a petri dish (Figure 2F). Meanwhile, supramolecular hydrogel (3.0 wt % LNSs, 0.5 wt % GC) could be extruded through a 23-gauge needle without clogging to form "ABC" hydrogels successfully (Figure2G). Similarly, different shaped molds were used to simulate irregular tissue defects (Figure 2H). The molds could be filled with extruded hydrogels using a 23-gauge needle to rebuild unabridged triangle-, oval-, heart-, and hexagon-shaped hydrogels, indicating that these non-covalently driven hydrogels have great potential for therapies of irregular tissue defects with minimally invasive approach due to their injectable performance.

To quantify the mechanical performance associated with shear-thinning and the subsequent recovery, we measured the rheological properties of the LNSs/GC hydrogels. The hydrogel with 3 wt % LNSs and 0.5 wt % GC had a storage modulus (G') of ~215 Pa and a loss modulus (G") of ~183 Pa as functions of angular frequency at a fixed strain, $\gamma = 5.0\%$ (Figure 3A). As shown in Figure 3B, strain sweeps of the hydrogels revealed an elastic response characters of hydrogels. The G' and G" values decreased fleetly at a critical shear stress level, indicating a collapse of hydrogels. Furthermore, cyclic high and low stresses were applied to the hydrogels (Figure 3C). At a low stress (1%) level, the value of G' was

higher than G", indicating that the hydrogel was stable. Once the stress increased to 300%, the value of G' was lower than G", demonstrating that the hydrogel was changed into a liquid-like state. After removing the high stress, the hydrogel was recovered immediately. The degradation of hydrogels was evaluated and displayed in Figure 3D. The weight of hydrogels with 3 wt % LNSs and 0.5 wt % GC decreased 48.4% and 45.2% after incubation for 40 days in PBS (pH 7.4) and culture medium, respectively.

3.2. Cytotoxicity and Osteoinduction of Hydrogels.

Once the expected self-healing and injectable features were verified successfully, both biocompatibility and osteoinductive capacity were evaluated using mouse bone marrow stromal cells (BMSCs).[47–50] BMSCs were cultured in tissue culture plates and exposed to the hydrogel samples. The viability of the cell cultures exposed to the hydrogels was not significantly different compared to untreated cells (Figure S6). Cell proliferation in hydrogel 3D culture using alamarBlue™ assay was shown in Figure 4A. There was no obvious difference in cell growth rate in hydrogels with different concentrations of LNSs from 2.5 to 4.5 wt %. The fluorescence intensity of hydrogel (LNSs = 3.0 wt %) increased to ~3.4 times at day 3 compared with day 1. The growth rate slowed down from day 3 to 7, maybe due to BMSCs that were directed to differentiation rather than proliferation. Moreover, we employed a Calcein AM and EthD-1 staining approach to distinguish live (green) and dead (red) cells (Figure S7 and Figure S8). The cells grew very well and there were no apparent dead cells after 7 days of culture, which agreed well with the alamarBlue™ staining results. Therefore, our supramolecular hydrogels display good biocompatibility and may act as a favorable substrate for cell growth and differentiation.

To further evaluate the osteogenic efficiency of the supramolecular hydrogels for bone regeneration, the activity and expression of ALP, an early marker of osteogenic differentiation, was first tested in BMSCs encapsulated with hydrogels.[47–50] As shown in Figure 4B, ALP activity revealed a significant increase at day 3 and reached the highest value at day 14. Hydrogels containing 4.5 wt % LNSs displayed 1.5-fold higher ALP activity than hydrogels containing 2.5 wt % LNSs. In contrast, increasing the amount of GC binder did not have a significant impact on ALP activity (Figure S9). ALP expression was also observed after staining with BCIP/NBT using a microscope directly (Figure 4C). Consistent with prior results of ALP activity, ALP expression increased over time and was significantly elevated in hydrogels with increased LNS concentration. Moreover, hydrogels displayed moderate osteogenic ability under basal culture medium (Figure S10). To assess mineralization (late osteogenic marker) in hydrogels, Alizarin red S was subsequently used to stain calcium (Figure 4D). Intense Alizarin red Stain was observed during 14 day culture, indicating deposition of calcium. Staining was more intense as the amount of LNSs increased. The quantification of calcium deposition shown that hydrogels with 4.0 wt % and 4.5 wt % LNSs displayed the highest values at all of the time points, which was consistent with the corresponding staining (Figure S11). The staining and quantitative data indicated the elevated osteogenic capacity resulting from inherent osteoinductivity of LNSs.

3.3. Osteogenic Gene Expression of Hydrogels.

To uncover the osteogenesis efficiency on molecular level, qPCR analysis was used to detect the level of osteogenic gene expression including *ALP* (a marker in the early stage), *Runx2* (an osteoblast-specific marker) and *OCN* (a marker in the later stage).[47–50] As exhibited in Figure 5A, hydrogels with increased amounts of LNSs had higher levels of *ALP*, *Runx2* and *OCN* expression at day 14 when compared with day 1. Of note, hydrogels with 4.5 wt % LNSs increased the level of *ALP* and *Runx2* to 1.6- and 1.9-fold respectively at day 14, and increased the level of *OCN* to 1.5-fold at day 21 when compared with hydrogels with 2.5 wt % LNSs. Overall, the increase of LNSs from 2.5 to 4.5 wt % could give rise to the considerable upregulation of osteogenic genes, consistent with the evidence for increased ALP and mineral accumulation. Given the Wnt/β-catenin signaling activation by the degradation products of lithium and orthosilicic acid from LNSs, the mRNA levels of several key proteins in Wnt/β-catenin signaling including Gsk3 and β-catenin were also determined using qPCR assay (Figure 5B).[51–52] The level of *β-catenin* in hydrogels with 3.0 wt % LNSs was increased up to 1.7-fold, while the levels of *Gsk3*, which negatively regulates β-catenin signal were decreased up to 0.42-fold at day 14. In addition, the mRNA levels of *Integrin α* and *Integrin β* were investigated to evaluate the cell adhesion induced by magnesium (Figure 5C). The levels of *Integrin α* and *Integrin β* were upregulated with the increased amounts of LNSs in hydrogels, and about 1.5-fold and 1.6-fold increase was detected in hydrogels containing 4.5 wt % LNSs as compared with hydrogels containing 2.5 wt % LNSs 2 at day 14. Together, these results suggested that supramolecular hydrogels composed of LNSs and GC could stimulate cell osteogenic differentiation through activating Wnt/β-catenin signaling and enhance cell adhesion mediated by their degradation products including lithium, orthosilicic acid and magnesium.

3.4. Properties of DBM-Loaded Hydrogels.

DBM has been widely used in clinical treatment of bone defects due to its inherent osteoconductivity and osteoinductivity derived from its growth factor and protein matrix components, such as type I collagen, bone morphogenetic protein-2 (BMP-2), and osteopontin (OPN).[53–54] However, more extensive use of DBM particles is limited in large defect areas due to difficulties in handling, concerns about particle migration, and insufficient bone formation capacity.[55–57] Although synthetic inert carriers such as glycerol and hyaluronic acid have been used in clinical applications, they are rapidly dissolved in a body and DBM particles may migrate out of the defect site.[58–59] This may induce severe inflammation and the desired localized effect of BMPs present in DBM may not manifest. Taking the above into account, we explored our supramolecular hydrogels as polymeric carriers for DBM, to enhance handling properties and osteogenic potential. Since LPN concentrations of 3 wt% or higher presented desired gelation time (<100 s) to rapidly entrap cells and bioactive components, 3 wt% LPNs were tested in the DBM-loaded hydrogels as a starting concentration. Hydrogels containing 3 wt % LNSs could be formed after the addition of 1.5 to 6.0 wt % DBM, and their gelation times (100 s) were similar to that of DBM-free hydrogels containing equal LNSs (Figure S12). To investigate their self-healing properties, hydrogels prepared using 3.0 wt % LNSs and 3.0 wt % DBM were treated with rhodamine B and methylene blue to obtain two different colored hydrogels (Figure 6A and Figure 6B). After intimate contact, pink and blue hydrogels were healed into a single

integrated hydrogel. Also, hydrogel samples cut into two pieces could merge into one piece and the integral hydrogel was stable in deionized water. These results indicated that the loading of DBM had no influence on the self-healing nature of hydrogels.

The injectable properties of DBM-loaded hydrogels were investigated by extruding the hydrogels into a petri dish, molds with various shapes, or aqueous environment. As shown in Figure 6C and Figure 6D, DBM-loaded hydrogels not only could be injected into deionized water without any breakage but also could be injected using a syringe to form “DBM” characters. Also, four kinds of molds were employed to imitate irregular tissue defect sites and were filled with DBM-loaded hydrogels (Figure 6E). The extruded hydrogel fragments were healed into an integral object holding the same shapes with the original molds. Picrosirius Red was employed to stain DBM distribution in supramolecular hydrogels. As shown in Figure 6F, DBM could be distributed in hydrogels uniformly, maintaining its own particle morphology. These results indicate that supramolecular hydrogels well maintained their injectability after loading with DBM, and thus could provide convenient delivery of DBM for clinical usage.

3.5. Osteogenic Ability of DBM-Loaded Hydrogels.

To explore the cytocompatibility and potential osteoinduction of DBM-loaded hydrogels, BMSCs were encapsulated and cell viability was assessed using alamarBlue™ assay (Figure 7A). The growth rate of cells in DBM-loaded hydrogels was similar to that of cells in DBM-free hydrogels after incubation in culture medium for 7 days. Hydrogels containing 3.0 wt % DBM showed the fastest growth rate with a 3.5-fold increase at day 3 as compared with day 1. The growth rate slowed from day 3 to 7, suggesting that hydrogels coupled with DBM not only provided a suitable 3D microenvironment for cell growth but also may induce osteogenic differentiation. Additionally, hematoxylin and eosin (H&E) stain showed that BMSCs cultured in DBM-free scaffolds exhibited homogenous cell proliferation with a spindle-like shape, while cells in DBM-loaded hydrogels proliferated primarily along the surface of DBM (Figure 7B). For the evaluation of osteogenic capability, both ALP activity and expression were investigated after incubation at days 3, 7, and 14. ALP activity per ng DNA was 10.74 μM/ng in hydrogels with 3.0 wt % DBM at day 14, while there was 8.74 μM ALP activity per ng DNA in DBM-free hydrogels (Figure 7C). There was higher ALP expression in hydrogels with 3.0 and 6.0 wt % DBM than hydrogels with 1.5 wt % DBM at day 7 (Figure 7D and Figure S13). Alizarin red S staining showed more mineralization in supramolecular hydrogels containing 3.0 and 6.0 wt % DBM after incubation for 14 days (Figure 7D, and Figure S14). Moreover, the levels of expression of osteogenic genes including *ALP*, *Runx2* and *OCN* were were measured by qPCR (Figure 7E). After treatment in osteogenic medium for 14 days, the mRNA level of *ALP* in hydrogels loaded with 3.0 wt % DBM was increased 3.6-fold compared with DBM-free hydrogels, and the level of *Runx2* in hydrogels with 3.0 and 6.0 wt% DBM was increased 2.5-fold and 2.6-fold, respectively. At day 21, the level of *OCN* increased 2.1-fold, 2.7-fold and 2.8-fold in hydrogels with 1.5, 3.0, and 6.0 wt % DBM, respectively, when compared with DBM-free hydrogels. These results collectively suggest that DBM could cooperatively stimulate osteogenesis induced by LNSs and our supramolecular hydrogels can serve as an effective delivery system for DBM. The data obtained from this study may not indicate the most optimal LPN+DBM

combination for osteoinduction. Further studies will be need to evaluate the dose-dependent effect of LPNs.

4. CONCLUSIONS

In summary, we have extended a new strategy on the development of supramolecular hydrogels to explore their use for inducing bone regeneration. These hydrogels could be prepared by a simple mixing procedure using LNSs and guanidine-rich polysaccharides, which create a 3-D network via salt-bridge formation by hydrogen bonding and electrostatic interaction. In particular, the created hydrogels with 3 wt % LNSs displayed self-healing and injectable properties that could facilitate, minimally invasive delivery to irregular defect sites and integration with surrounding tissues. Moreover, the hydrogel showed inherent osteogenic properties by activating the Wnt/β-catenin signaling pathway without the addition of exogenous growth factors. Lastly, the supramolecular hydrogel system was effective to deliver DBM and could serve as a versatile moldable vehicle, facilitating handling and osteogenic potential. This work demonstrates a novel therapeutic supramolecular design that can create injectable and self-healing polymer networks with high osteoinductivity. The supramolecular hydrogel presents a versatile platform for encapsulating cells, therapeutic agents, and synthetic carriers for malleable bone graft constructs to promote clinical bone repair.

Supplementary Material

Refer to Web version on PubMed Central for supplementary material.

ACKNOWLEDGMENT

This work was supported by grants from the National Institutes of Health (R01 DE027332), the Department of Defense (W81XWH-18-1-0337), and the MTF Biologics.

REFERENCES

1. Moroni L; Burdick JA; Highley C; Lee SJ; Morimoto Y; Takeuchi S; Yoo JJ Biofabrication strategies for 3D in vitro models and regenerative medicine. Nat. Rev. Mater 2018, 3, 21–37. [PubMed: 31223488]
2. Balakrishnan B; Banerjee R Biopolymer-Based Hydrogels for Cartilage Tissue Engineering. Chem. Rev 2011, 111, 4453–4474. [PubMed: 21417222]
3. Hoffman AS Hydrogels for biomedical applications. Adv. Drug. Deliver. Rev 2012, 64, 18–23.
4. Lee KY; Mooney DJ Hydrogels for Tissue Engineering. Chem. Rev 2001, 101, 1869–1880. [PubMed: 11710233]
5. Peppas NA; Hilt JZ; Khademhosseini A; Langer R Hydrogels in Biology and Medicine: From Molecular Principles to Bionanotechnology. Adv. Mater 2006, 18, 1345–1360.
6. Slaughter BV; Khurshid SS; Fisher OZ; Khademhosseini A; Peppas NA Hydrogels in Regenerative Medicine. Adv. Mater 2009, 21, 3307–3329. [PubMed: 20882499]
7. Liu M; Zeng X; Ma C; Yi H; Ali Z; Mou X; Li S; Deng Y; He N Injectable hydrogels for cartilage and bone tissue engineering. Bone Res. 2017, 5, 17014. [PubMed: 28584674]
8. Yu L; Ding J Injectable hydrogels as unique biomedical materials. Chem. Soc. Rev 2008, 37, 1473–1481. [PubMed: 18648673]
9. Hennink WE; van Nostrum CF Novel crosslinking methods to design hydrogels. Adv. Drug. Deliver. Rev 2012, 64, 223–236.

10. Du X; Zhou J; Shi J; Xu B Supramolecular Hydrogelators and Hydrogels: From Soft Matter to Molecular Biomaterials. Chem. Rev 2015, 115, 13165–13307. [PubMed: 26646318]
11. Appel EA; del Barrio J; Loh XJ; Scherman OA Supramolecular polymeric hydrogels. Chem. Soc. Rev 2012, 41, 6195–6214. [PubMed: 22890548]
12. Chen H; Yang F; Chen Q; Zheng J A Novel Design of Multi-Mechanoresponsive and Mechanically Strong Hydrogels. Adv. Mater 2017, 29, 1606900.
13. Costa SA; Simon JR; Amiram M; Tang L; Zauscher S; Brustad EM; Isaacs FJ; Chilkoti A Photo-Crosslinkable Unnatural Amino Acids Enable Facile Synthesis of Thermoresponsive Nano- to Microgels of Intrinsically Disordepink Polypeptides. Adv. Mater 2018, 30, 1704878.
14. Ouyang L; Highley CB; Sun W; Burdick JA A Generalizable Strategy for the 3D Bioprinting of Hydrogels from Nonviscous Photo-crosslinkable Inks. Adv. Mater 2017, 29, 1604983.
15. Dou X-Q; Feng C-L Amino Acids and Peptide-Based Supramolecular Hydrogels for Three-Dimensional Cell Culture. Adv. Mater 2017, 29, 1604062.
16. Miyamae K; Nakahata M; Takashima Y; Harada A Self-Healing, Expansion–Contraction, and Shape-Memory Properties of a Preorganized Supramolecular Hydrogel through Host–Guest Interactions. Angew. Chem. Int. Edit 2015, 54, 8984–8987.
17. Voorhaar L; Hoogenboom R Supramolecular polymer networks: hydrogels and bulk materials. Chem. Soc. Rev 2016, 45, 4013–4031. [PubMed: 27206244]
18. Hu X; Vatankhah-Varnoosfaderani M; Zhou J; Li Q; Sheiko SS Weak Hydrogen Bonding Enables Hard, Strong, Tough, and Elastic Hydrogels. Adv. Mater 2015, 27, 6899–6905. [PubMed: 26436409]
19. Dawson JI; Kanczler JM; Yang XB; Attard GS; Oreffo ROC Clay Gels For the Delivery of Regenerative Microenvironments. Adv. Mater 2011, 23, 3304–3308. [PubMed: 21661063]
20. Dawson JI; Oreffo ROC Clay: New Opportunities for Tissue Regeneration and Biomaterial Design. Adv. Mater 2013, 25, 4069–4086. [PubMed: 23722321]
21. Han L; Lu X; Liu K; Wang K; Fang L; Weng L-T; Zhang H; Tang Y; Ren F; Zhao C; Sun G; Liang R; Li Z Mussel-Inspired Adhesive and Tough Hydrogel Based on Nanoclay Confined Dopamine Polymerization. ACS Nano 2017, 11, 2561–2574. [PubMed: 28245107]
22. Laurenti M; Al Subaie A; Abdallah M-N; Cortes ARG; Ackerman JL; Vali H; Basu K; Zhang YL; Murshed M; Strandman S; Zhu J; Makhoul N; Barralet JE; Tamimi F Two-Dimensional Magnesium Phosphate Nanosheets Form Highly Thixotropic Gels That Up-Regulate Bone Formation. Nano. Lett 2016, 16, 4779–4787. [PubMed: 27280476]
23. Tomás H; Alves CS; Rodrigues J Laponite®: A key nanoplatform for biomedical applications? Nanomed.-Nanotechnol 2018, 14, 2407–2420.
24. Hedgepeth CM; Conrad LJ; Zhang J; Huang H-C; Lee VMY; Klein PS Activation of the Wnt Signaling Pathway: A Molecular Mechanism for Lithium Action. Dev. Biol 1997, 185, 82–91. [PubMed: 9169052]
25. Han P; Wu C; Xiao Y The effect of silicate ions on proliferation, osteogenic differentiation and cell signalling pathways (WNT and SHH) of bone marrow stromal cells. Biomater. Sci 2013, 1, 379–392.
26. Luthringer BJC; Willumeit-Römer R Effects of magnesium degradation products on mesenchymal stem cell fate and osteoblastogenesis. Gene 2016, 575, 9–20. [PubMed: 26283150]
27. Zhang F; Phiel CJ; Spece L; Gurvich N; Klein PS Inhibitory Phosphorylation of Glycogen Synthase Kinase-3 (GSK-3) in Response to Lithium: EVIDENCE FOR AUTOREGULATION OF GSK-3. J. Biol. Chem 2003, 278, 33067–33077. [PubMed: 12796505]
28. Clément-Lacroix P; Ai M; Morvan F; Roman-Roman S; Vayssière B; Belleville C; Estrera K; Warman ML; Baron R; Rawadi G Lrp5-independent activation of Wnt signaling by lithium chloride increases bone formation and bone mass in mice. Proc. Natl. Acad. Sci. USA 2005, 102, 17406–17411. [PubMed: 16293698]
29. Yoshizawa S; Brown A; Barchowsky A; Sfeir C Magnesium ion stimulation of bone marrow stromal cells enhances osteogenic activity, simulating the effect of magnesium alloy degradation. Acta Biomater. 2014, 10, 2834–2842. [PubMed: 24512978]

30. Zhang J; Ma X; Lin D; Shi H; Yuan Y; Tang W; Zhou H; Guo H; Qian J; Liu C Magnesium modification of a calcium phosphate cement alters bone marrow stromal cell behavior via an integrin-mediated mechanism. Biomaterials 2015, 53, 251–264. [PubMed: 25890724]

31. Xavier JR; Thakur T; Desai P; Jaiswal MK; Sears N; Cosgriff-Hernandez E; Kaunas R; Gaharwar AK Bioactive Nanoengineepink Hydrogels for Bone Tissue Engineering: A Growth-Factor-Free Approach. ACS Nano 2015, 9, 3109–3118. [PubMed: 25674809]

32. Gaharwar AK; Mihaila SM; Swami A; Patel A; Sant S; Reis RL; Marques AP; Gomes ME; Khademhosseini A Bioactive Silicate Nanoplatelets for Osteogenic Differentiation of Human Mesenchymal Stem Cells. Adv. Mater 2013, 25, 3329–3336. [PubMed: 23670944]

33. Gaharwar AK; Kishore V; Rivera C; Bullock W; Wu C-J; Akkus O; Schmidt G Physically Crosslinked Nanocomposites from Silicate-Crosslinked PEO: Mechanical Properties and Osteogenic Differentiation of Human Mesenchymal Stem Cells. Macromol. Biosci 2012, 12, 779–793. [PubMed: 22517665]

34. Yao C; Liu Z; Yang C; Wang W; Ju X-J; Xie R; Chu L-Y Smart Hydrogels with Inhomogeneous Structures Assembled Using Nanoclay-Cross-Linked Hydrogel Subunits as Building Blocks. ACS Appl. Mater. & Inter 2016, 8, 21721–21730.

35. Choi J.-y.; Ryu K; Lee GJ; Kim K; Kim T.-i. Agmatine-Containing Bioreducible Polymer for Gene Delivery Systems and Its Dual Degradation Behavior. Biomacromolecules 2015, 16, 2715–2725. [PubMed: 26252660]

36. Kim T.-i.; Lee M; Kim SW A guanidinylated biopinkucible polymer with high nuclear localization ability for gene delivery systems. Biomaterials 2010, 31, 1798–1804. [PubMed: 19854504]

37. Wender PA; Rothbard JB; Jessop TC; Kreider EL; Wylie BL Oligocarbamate Molecular Transporters: Design, Synthesis, and Biological Evaluation of a New Class of Transporters for Drug Delivery. J. Am. Chem. Soc 2002, 124, 13382–13383. [PubMed: 12418880]

38. Lee JH; Kim C; Jung JH Control of the rheological properties of clay nanosheet hydrogels with a guanidinium-attached calix[4]arene binder. Chem. Commun 2015, 51, 15184–15187.

39. Wang Q; Mynar JL; Yoshida M; Lee E; Lee M; Okuro K; Kinbara K; Aida T High-water-content mouldable hydrogels by mixing clay and a dendritic molecular binder. Nature 2010, 463, 339–343. [PubMed: 20090750]

40. Tamesue S; Ohtani M; Yamada K; Ishida Y; Spruell JM; Lynd NA; Hawker CJ; Aida T Linear versus Dendritic Molecular Binders for Hydrogel Network Formation with Clay Nanosheets: Studies with ABA Triblock Copolyethers Carrying Guanidinium Ion Pendants. J. Am. Chem. Soc 2013, 135, 15650–15655. [PubMed: 24050260]

41. Li Z; Zhang Y-M; Wang H-Y; Li H; Liu Y Mechanical Behaviors of Highly Swollen Supramolecular Hydrogels Mediated by Pseudorotaxanes. Macromolecules 2017, 50, 1141–1146.

42. Yang X; Liu G; Peng L; Guo J; Tao L; Yuan J; Chang C; Wei Y; Zhang L Highly Efficient Self-Healable and Dual Responsive Cellulose-Based Hydrogels for Controlled Release and 3D Cell Culture. Adv. Funct. Mater 2017, 27, 1703174.

43. Wei Z; Yang JH; Liu ZQ; Xu F; Zhou JX; Zrínyi M; Osada Y; Chen YM Novel Biocompatible Polysaccharide-Based Self-Healing Hydrogel. Adv. Funct. Mater 2015, 25, 1352–1359.

44. Basu S; Pacelli S; Feng Y; Lu Q; Wang J; Paul A Harnessing the Noncovalent Interactions of DNA Backbone with 2D Silicate Nanodisks To Fabricate Injectable Therapeutic Hydrogels. ACS Nano 2018, 12, 9866–9880. [PubMed: 30189128]

45. Tseng T-C; Tao L; Hsieh F-Y; Wei Y; Chiu I-M; Hsu S-h. An Injectable, Self-Healing Hydrogel to Repair the Central Nervous System. Adv. Mater 2015, 27, 3518–3524. [PubMed: 25953204]

46. Rodell CB; MacArthur JW Jr.; Dorsey SM; Wade RJ; Wang LL; Woo YJ; Burdick JA Shear-Thinning Supramolecular Hydrogels with Secondary Autonomous Covalent Crosslinking to Modulate Viscoelastic Properties In Vivo. Adv. Funct. Mater 2015, 25, 636–644. [PubMed: 26526097]

47. Kim S; Cui Z-K; Koo B; Zheng J; Aghaloo T; Lee M Chitosan–Lysozyme Conjugates for Enzyme-Triggered Hydrogel Degradation in Tissue Engineering Applications. ACS Appl. Mater. & Inter 2018, 10, 41138–41145.

48. Cui Z-K; Kim S; Baljon JJ; Doroudgar M; Lafleur M; Wu BM; Aghaloo T; Lee M Design and Characterization of a Therapeutic Non-phospholipid Liposomal Nanocarrier with Osteoinductive

Characteristics To Promote Bone Formation. ACS Nano 2017, 11, 8055–8063. [PubMed: 28787576]

49. Cui Z-K; Kim S; Baljon JJ; Wu BM; Aghaloo T; Lee M Microporous methacrylated glycol chitosan-montmorillonite nanocomposite hydrogel for bone tissue engineering. Nat. Commun 2019, 10, 3523. [PubMed: 31388014]
50. Cui Z-K; Sun JA; Baljon JJ; Fan J; Kim S; Wu BM; Aghaloo T; Lee M Simultaneous delivery of hydrophobic small molecules and siRNA using Sterosomes to direct mesenchymal stem cell differentiation for bone repair. Acta Biomater. 2017, 58, 214–224. [PubMed: 28578107]
51. Kahn M Can we safely target the WNT pathway? Nat. Rev. Drug. Discov 2014, 13, 513–532. [PubMed: 24981364]
52. Cohen P; Goedert M GSK3 inhibitors: development and therapeutic potential. Nat. Rev. Drug. Discov 2004, 3, 479–487. [PubMed: 15173837]
53. Holt DJ; Grainger DW Demineralized bone matrix as a vehicle for delivering endogenous and exogenous therapeutics in bone repair. Adv. Drug. Deliver. Rev 2012, 64, 1123–1128.
54. Song JJ; Ott HC Organ engineering based on decellularized matrix scaffolds. Trends Mol Med 2011, 17, 424–432. [PubMed: 21514224]
55. Shi J; Sun J; Zhang W; Liang H; Shi Q; Li X; Chen Y; Zhuang Y; Dai J Demineralized Bone Matrix Scaffolds Modified by CBD-SDF-1α Promote Bone Regeneration via Recruiting Endogenous Stem Cells. ACS Appl. Mater. & Inter 2016, 8, 27511–27522.
56. Hu Q; Liu M; Chen G; Xu Z; Lv Y Demineralized Bone Scaffolds with Tunable Matrix Stiffness for Efficient Bone Integration. ACS Appl. Mater. & Inter 2018, 10, 27669–27680.
57. Gupta V; Lyne DV; Laflin AD; Zabel TA; Barragan M; Bunch JT; Pacicca DM; Detamore MS Microsphere-Based Osteochondral Scaffolds Carrying Opposing Gradients Of Decellularized Cartilage And Demineralized Bone Matrix. ACS Biomaterials Science & Engineering 2017, 3, 1955–1963.
58. Zheng Y; Huang K; You X; Huang B; Wu J; Gu Z Hybrid hydrogels with high strength and biocompatibility for bone regeneration. Int J Biol Macromol 2017, 104, 1143–1149. [PubMed: 28687387]
59. Man Z; Hu X; Liu Z; Huang H; Meng Q; Zhang X; Dai L; Zhang J; Fu X; Duan X; Zhou C; Ao Y Transplantation of allogenic chondrocytes with chitosan hydrogel-demineralized bone matrix hybrid scaffold to repair rabbit cartilage injury. Biomaterials 2016, 108, 157–167. [PubMed: 27636153]

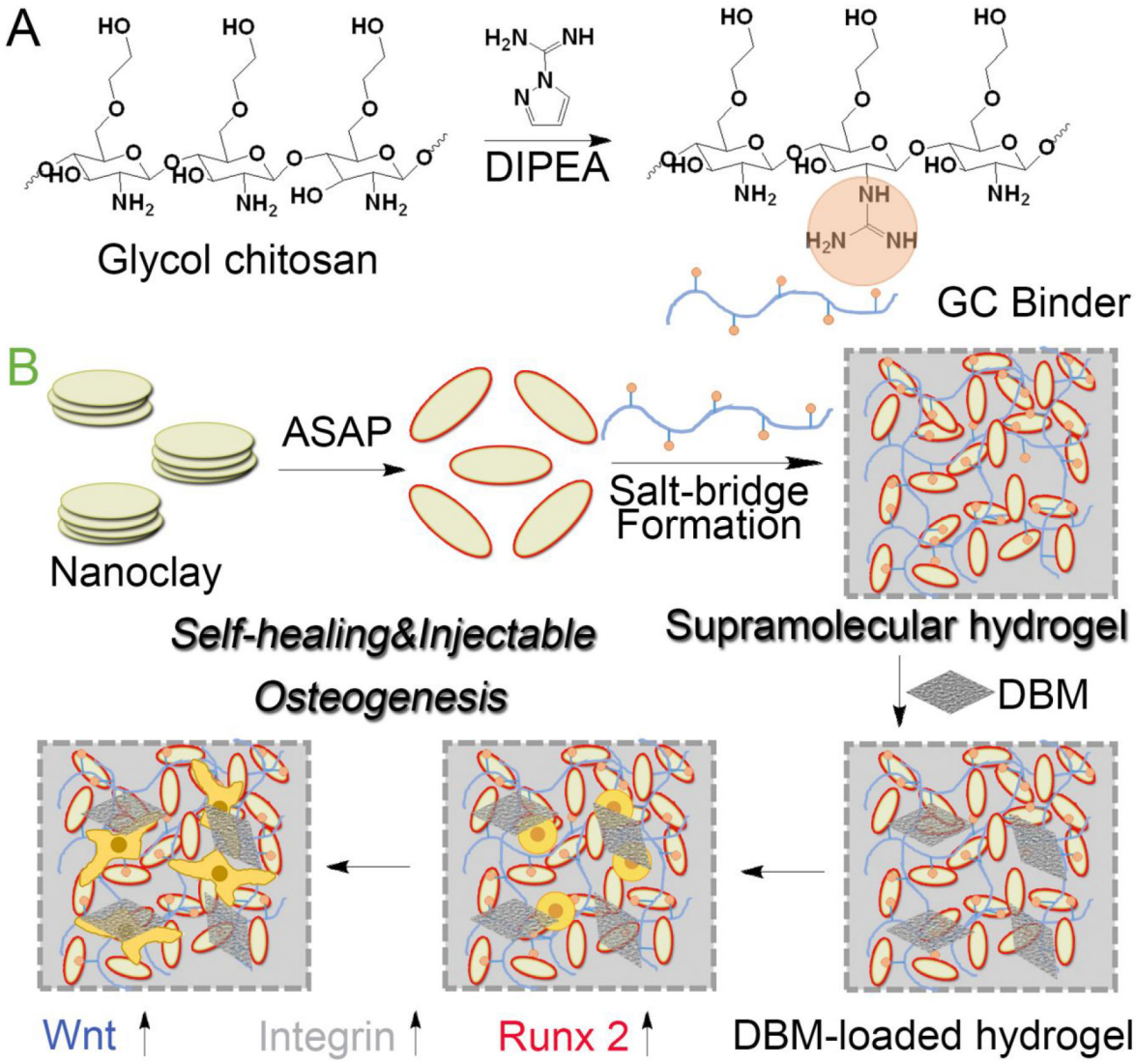

Figure 1.

Schematic illustration of supramolecular hydrogels with self-healing and injectable properties for bone regeneration with no need for growth factors, including (A) guanidine modification of glycol chitosan to obtain GC binder, (B) preparation of supramolecular hydrogel based on nanoclay and GC binder via salt-bridge formation by hydrogen bonding and electrostatic interaction, DBM loading and stem cell osteogenic differentiation along with activation of Wnt/β-catenin signaling and promotion of cell adhesion.

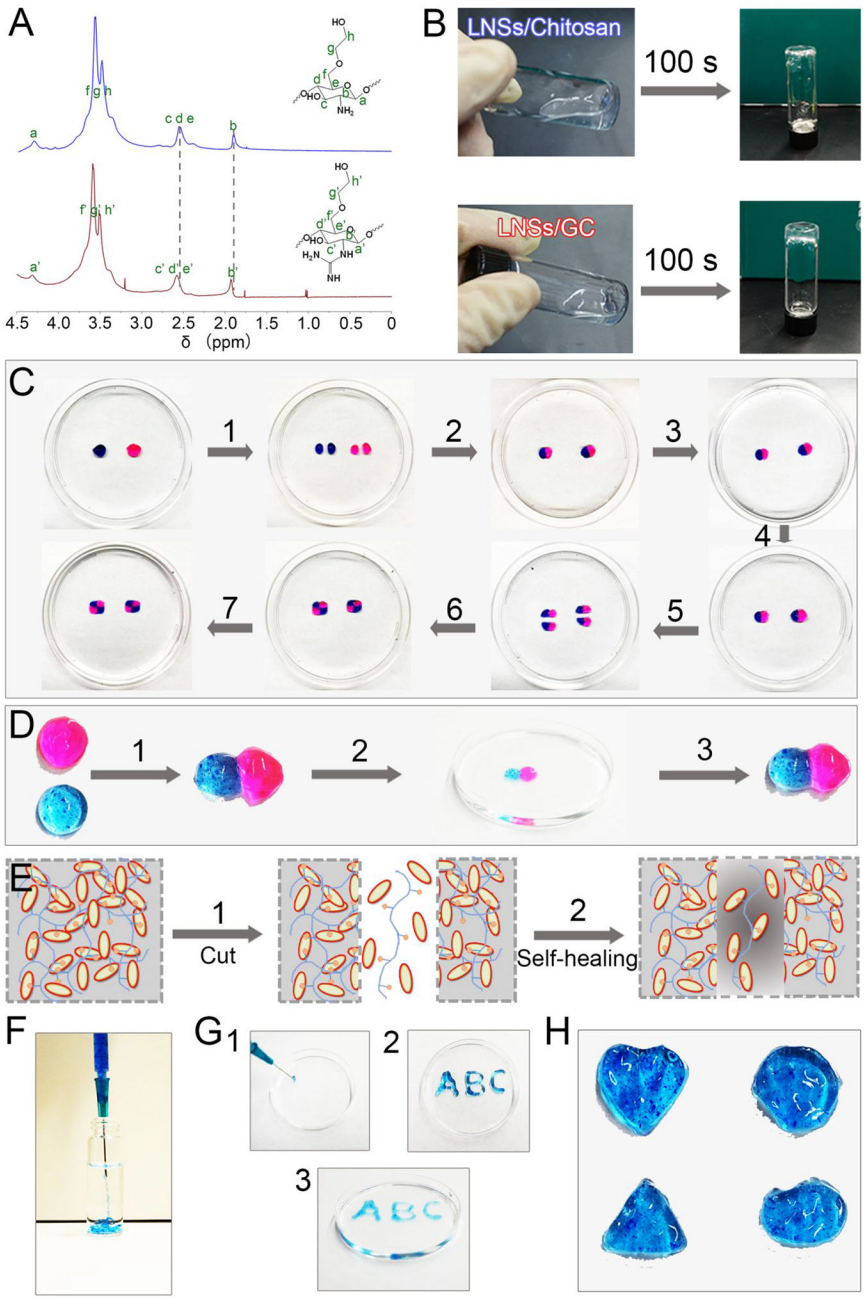

Figure 2.

Physical and chemical properties of supramolecular hydrogels. (A) ^{1}H NMR spectra of the glycol chitosan (blue line) and GC binder (red) in D_2O. (B) Images of LNSs with glycol chitosan and LNSs with GC binder. (C) Self-healing processes of supramolecular hydrogels: (1) two disk-shaped hydrogels stained with rhodamine B and methylene blue were cut into equal two pieces; (2) one piece of pink hydrogel and one piece of blue hydrogel were joined together to form two new hydrogels; (3) these two new hydrogels were immersed in PBS; (4) PBS was removed after 3 h; (5) these two new hydrogels were re-cut into equal two pieces; (6) two pieces of pink-blue hydrogels were joined together to form two new

hydrogels; (7) these two new hydrogels were immersed in PBS again. (D) Self-healing of two hydrogels after attachment directly: (1) pink hydrogel and blue hydrogel were attached directly; (2) the new hydrogel was immersed into deionized water for 10 min; (3) the hydrogel was transferred from deionized water and maintained its shape. (E) Scheme diagram of the self-healing process. (F) Images of hydrogels injected from 23 G needle into water. (G) “ABC” gel could be formed after injection from 23 G needle. (H) Hydrogels with different shape could be obtained after injection from 23 G needle.

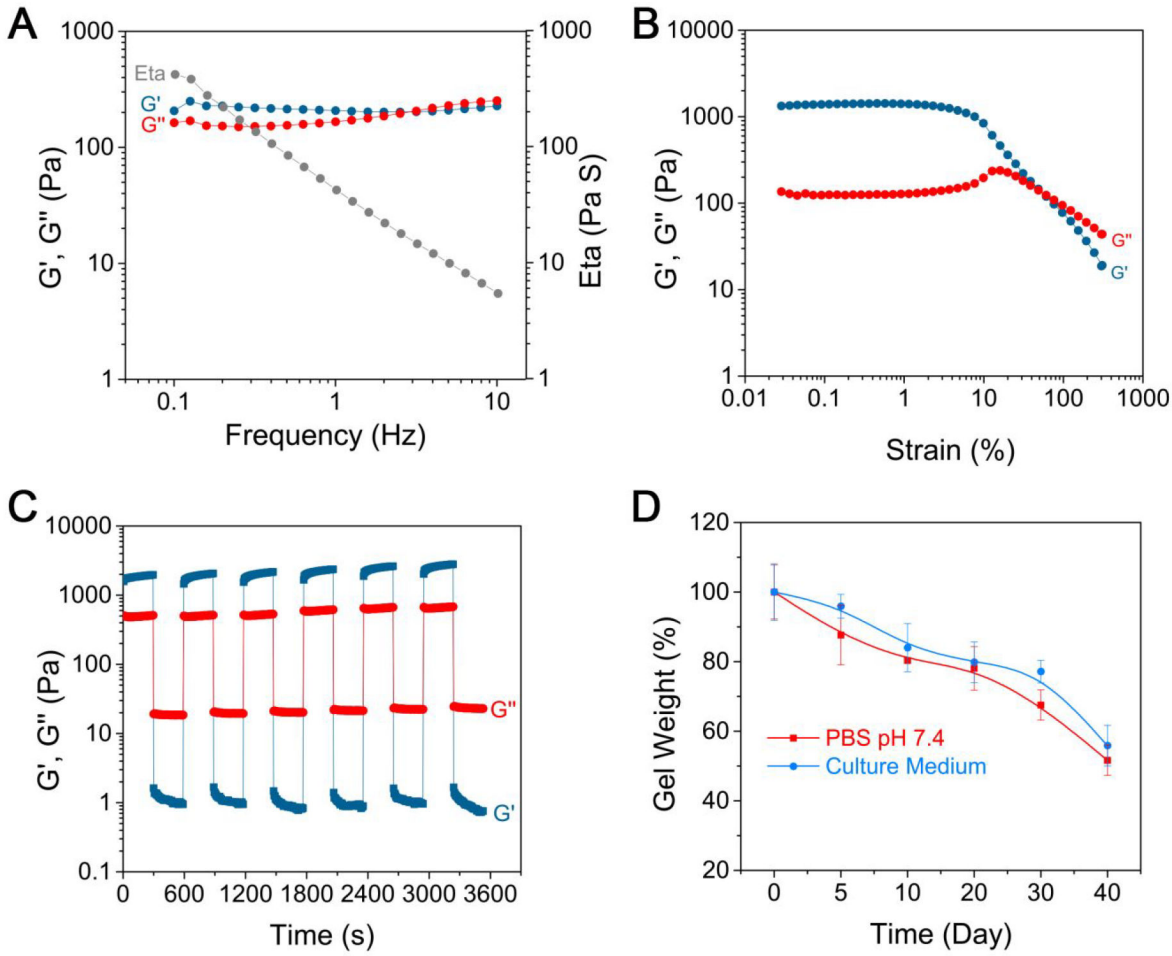

Figure 3.

Rheological and degradation properties of supramolecular hydrogels. (A) G', G" and Eta values of hydrogels with 3.0 wt % LNSs on frequency sweep at γ = 5.0%. G' and G" values of hydrogels with 3.0 wt % LNSs on strain sweep at frequency = 1.6 Hz. (B) and in continuous step strain measurements (C). (D) Degradation kinetics of hydrogels in PBS and culture medium for 40 days by measuring the weight.

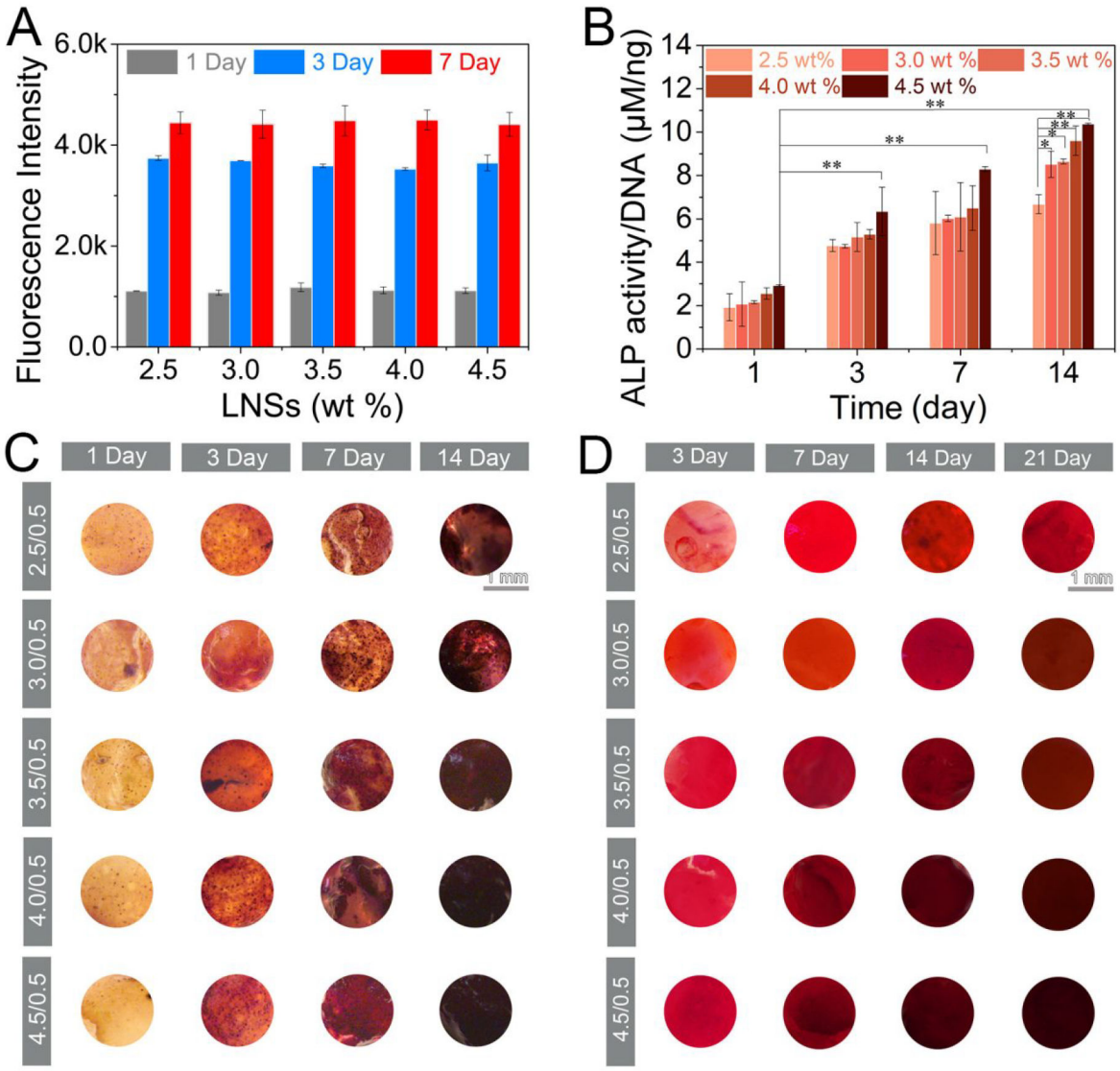

Figure 4.

Osteoinductive efficiency of supramolecular hydrogels. (A) Fluorescence intensity of alamarBlue towards MSCs after incubation in culture medium for 1, 3 and 7 days (n=3). (B) ALP activity (n=3, *$p < 0.05$, **$p < 0.001$ by one-way analysis of variance, ANOVA) and (C) ALP expression of cell-encapsulated hydrogels with LNSs ranging from 2.5 to 4.5 wt % treated in osteogenic medium for 1, 3, 7 and 14 days. Scar bar repents 1 mm. (D) Mineralization of cell-encapsulated hydrogels with LNSs ranging from 2.5 to 4.5 wt % after incubation with osteogenic medium for 3, 7, 14 and 21 days. Scar bar repents 1 mm.

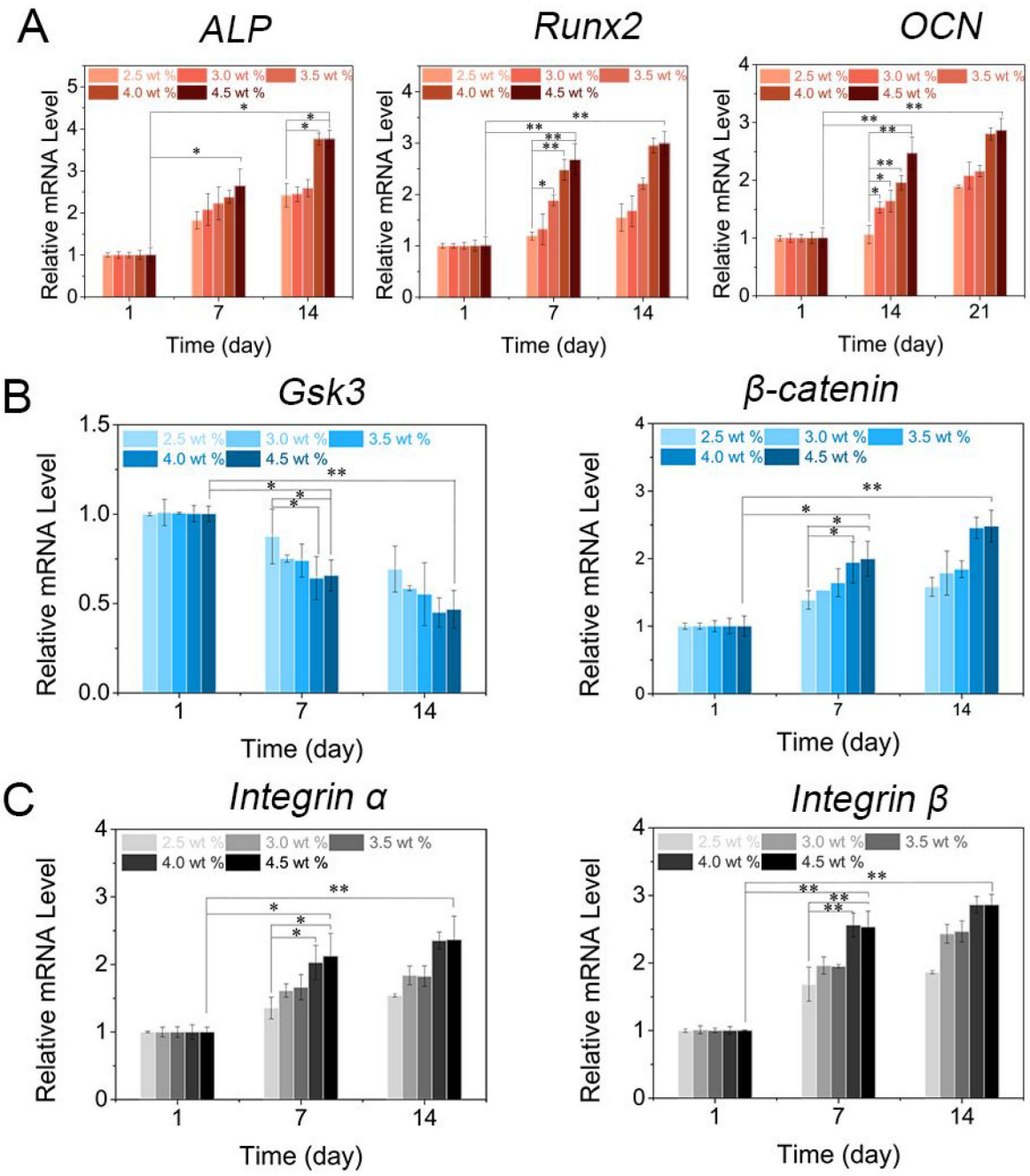

Figure 5.

Gene expression of cell-encapsulated supramolecular hydrogels. (A) Osteogenic genes *ALP* and *Runx2* were tested at day 1, 7 and 14. *OCN* was evaluated at day 1, 14 and 21 (n=3, *p < 0.05, **p < 0.001 by one-way analysis of variance, ANOVA). (B) Wnt/β-catenin signaling markers *Gsk3* and *β-catenin* and (C) cell adhesion markers *Integrin α* and *Integrin β* were evaluated after incubation for 1, 7 and 14 days (n=3, *p < 0.05, **p < 0.001by one-way analysis of variance, ANOVA).

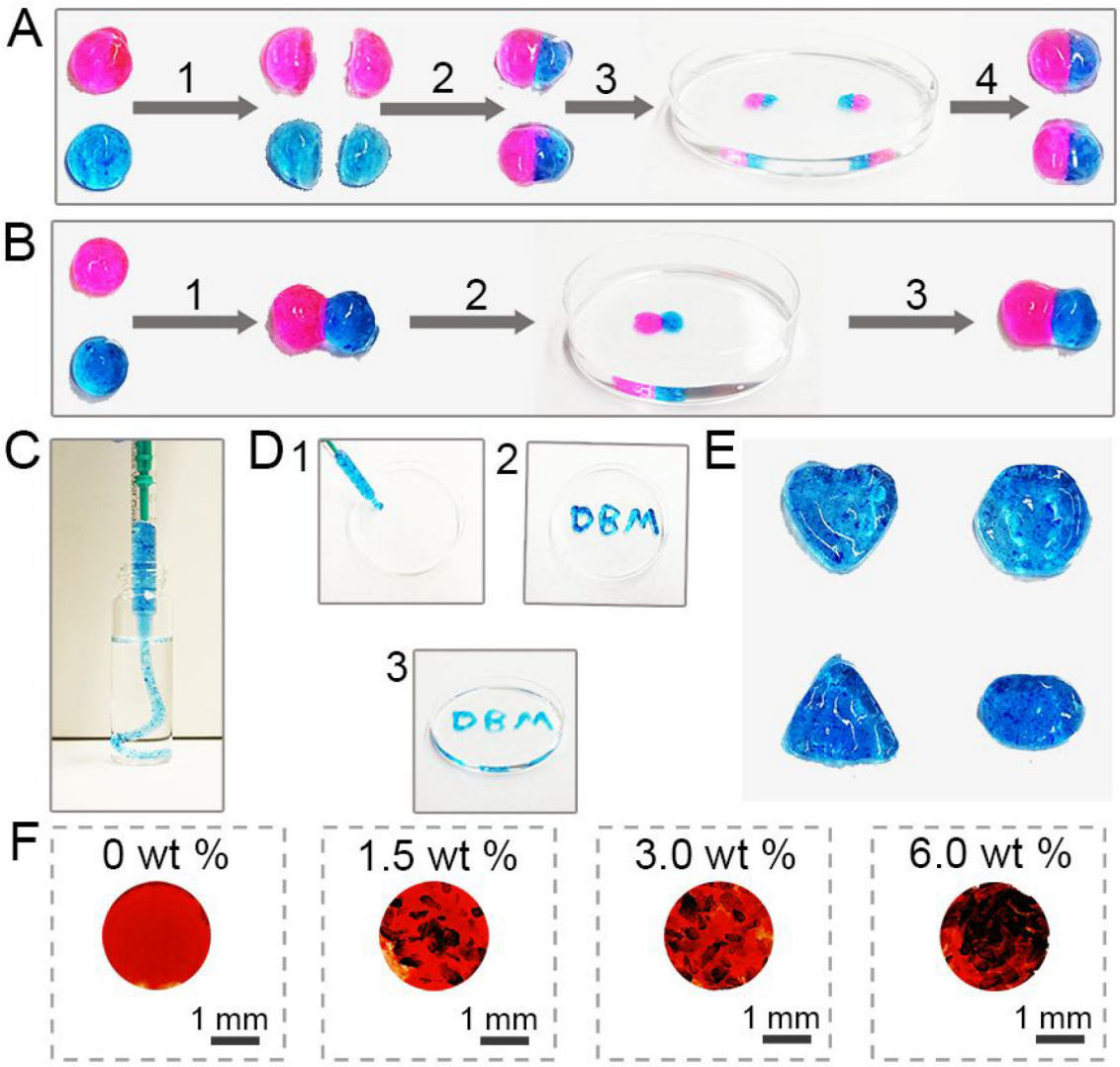

Figure 6.

Physical and chemical properties of DBM-loaded hydrogels. (A) Self-healing processes of DBM-loaded supramolecular hydrogels: (1) two disk-shaped DBM-loaded hydrogels stained with rhodamine B and methylene blue were cut into equal two pieces; (2) one piece of pink hydrogel and one piece of blue hydrogel were joined together to form two new hydrogels; (3) These two new hydrogels were immersed in deionized water for 10 min; (4) the hydrogels were transferred from deionized water. (B) Self-healing of two DBM-loaded hydrogels after attachment directly: (1) pink hydrogel and blue hydrogel were attached directly; (2) the new hydrogel was immersed into deionized water for 10 min; (3) the hydrogel was transferred from deionized water and maintained its shape. (C) Images of DBM-loaded hydrogels injected from a syringe without needle into water. (D) “DBM” gel could be formed after injection from a syringe without needle. (E) Hydrogels with different shapes could be obtained after injection from a syringe without needle. (F) Images of hydrogels and DBM-loaded hydrogels after staining with Picrosirius Red.

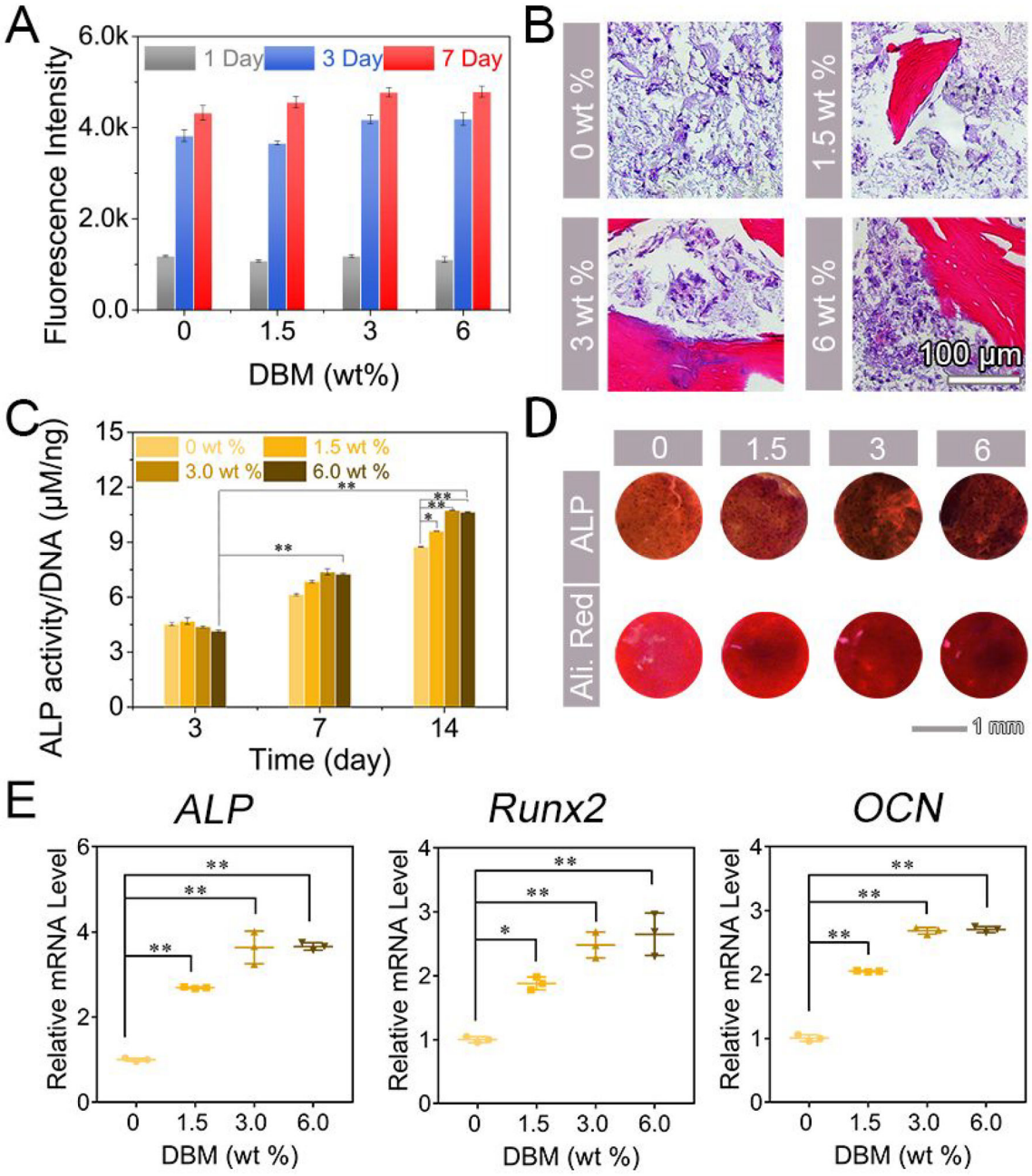

Figure 7.

Osteoinductive efficiency of DBM-loaded hydrogels. (A) Fluorescence intensity of alamarBlue™ towards cell-encapsulated DBM-loaded hydrogels after incubation in culture medium for 1, 3 and 7 days (n=3). (B) Histological images for H&E staining of cell-encapsulated DBM-loaded hydrogels after incubation in osteogenic medium for 21 days. Scar bar repents 100 μm. (C) ALP activity of cell-encapsulated DBM-loaded hydrogels treated in osteogenic medium for 3, 7 and 14 days (n=3, *p < 0.05, **p < 0.001 by one-way analysis of variance, ANOVA). (D) ALP expression DBM-loaded hydrogels in osteogenic medium for 7 days and mineralization of cell-encapsulated DBM-loaded hydrogels after incubation with osteogenic medium for 14 days. Scar bar repents 1 mm. (E) mRNA levels of

ALP and *Runx2* at day 14 and *OCN* at day 21 (n=3, *p < 0.05, **p < 0.001by one-way analysis of variance, ANOVA).